Deforestation Impacts on Clouds and Precipitation Over Borneo Vary Across the Diurnal Cycle

Gabrielle "Bee" Leung[1] and Susan C van den Heever[2]

[1]University of Wisconsin - Madison
[2]Colorado State University

October 10, 2025

Abstract

The impact of tropical deforestation on clouds and precipitation remains uncertain due to complex interactions between land surface changes and atmospheric processes on convective and mesoscales. Here, we examine the impact of deforestation over Borneo in Southeast Asia using a pair of high-resolution large eddy simulations. Replacing tropical forest with oil palm plantations reduces surface roughness thereby making surface-atmosphere exchanges less efficient, leading to warmer land but a cooler near-surface atmosphere. In this moist environment, evapotranspiration can compensate for the added surface heating, thereby increasing local moisture availability. To examine how this impacts cloud formation, we identify and track tens of thousands of clouds to quantify shifts in the distribution of tropical convection across the diurnal cycle. Overall, deforestation suppresses shallow-to-deep convective development, though the shallow cumuli which do form start raining earlier in the day due to increased low-level moisture. However, this reduction in shallow cloud cover is not spatially uniform: in areas where the deforestation gradient is strong, midday shallow cumuli are enhanced by mesoscale vegetation breezes. Deforestation also weakens sea breeze-driven moisture convergence, leading to the relative enhancement of terminal congestus over deep convection and a shift in the onset of deep convection and precipitation towards later in the evening. Our findings emphasize that deforestation impacts can vary diurnally depending on cloud type and interactions with mesoscale phenomena, as well as spatially depending on the location relative to deforested regions. This variability should be incorporated when considering the overall impact of deforestation on clouds, rainfall, and climate.

Deforestation Impacts on Clouds and Precipitation Over Borneo Vary Across the Diurnal Cycle

G. Leung[1,2], and S.C. van den Heever[1]

[1]Department of Atmospheric Science, Colorado State University

[2]Department of Atmospheric and Oceanic Sciences, University of Wisconsin – Madison

Corresponding author: Gabrielle "Bee" Leung (bee.leung@wisc.edu)

CRediT author contributions:

G.L. – Conceptualization, Funding acquisition, Formal analysis, Methodology, Software, Visualization, Writing – original draft

S.C.v.d.H. – Conceptualization, Funding acquisition, Supervision, Resources, Writing – review & editing

Key Points:

- Vegetation shifts from forest to oil palms lowers sensible heating and raises latent heating as evapotranspiration offsets surface warming.
- Deforestation decreases shallow cloud cover but enhances cloudiness along deforestation boundaries via vegetation breezes.
- Deforestation weakens the moisture convergence driving sea breeze deep convective rainfall but shallow cumuli rain earlier in the day.

Abstract

The impact of tropical deforestation on clouds and precipitation remains uncertain due to complex interactions between land surface changes and atmospheric processes on convective and mesoscales. Here, we examine the impact of deforestation over Borneo in Southeast Asia using a pair of high-resolution large eddy simulations. Replacing tropical forest with oil palm plantations reduces surface roughness thereby making surface-atmosphere exchanges less efficient, leading to warmer land but a cooler near-surface atmosphere. In this moist environment, evapotranspiration can compensate for the added surface heating, thereby increasing local moisture availability. To examine how this impacts cloud formation, we identify and track tens of thousands of clouds to quantify shifts in the distribution of tropical convection across the diurnal cycle. Overall, deforestation suppresses shallow-to-deep convective development, though the shallow cumuli which do form start raining earlier in the day due to increased low-level moisture. However, this reduction in shallow cloud cover is not spatially uniform: in areas where the deforestation gradient is strong, midday shallow cumuli are enhanced by mesoscale vegetation breezes. Deforestation also weakens sea breeze-driven moisture convergence, leading to the relative enhancement of terminal congestus over deep convection and a shift in the onset of deep convection and precipitation towards later in the evening. Our findings emphasize that deforestation impacts can vary diurnally depending on cloud type and interactions with mesoscale phenomena, as well as spatially depending on the location relative to deforested regions. This variability should be incorporated when considering the overall impact of deforestation on clouds, rainfall, and climate.

Plain Language Summary

Deforestation is widespread in the tropics. Though we know changes to the land surface can impact the atmosphere above it, we still do not fully understand how these changes affect different types of clouds throughout the day. Here, we use an atmospheric model to simulate clouds over Southeast Asia. We explore how deforestation impacts cloud formation by comparing simulations with the same atmospheric conditions but using pre- and post-deforestation land cover. Most crucially, we find deforestation can have contrasting impacts on cloudiness depending on the time of day and spatial scale. Deforestation slows the transition of shallow clouds into deep convection. However, it locally increases cloudiness close to the deforestation boundary by driving breezes between the forest and deforested areas. The impacts of deforestation on rainfall are similarly complex, with increases in area covered by weak rain but a large decrease in rainfall amounts overall. These findings show that the impact of deforestation on clouds and rainfall is not simple. The atmospheric response to forest loss depends on many competing processes that need to be considered if we want to accurately predict how deforestation impacts freshwater availability, precipitation extremes, and the climate and hydrology of tropical regions.

1 Introduction

Anthropogenic activities drive widespread deforestation in the tropics (Kim et al., 2015; Winkler et al., 2021). Southeast Asia—particularly the island of Borneo—is a hotspot of tropical deforestation, with extensive forest clearing in recent decades driven primarily by oil palm and rubber plantations (S. Chen et al., 2024; Jamaludin et al., 2022; Parker et al., 2024). It is widely accepted that these changes to land surface properties impact the atmosphere through their effects on fluxes of heat, moisture, and momentum between the surface and atmosphere (Mahmood et al., 2014; Santanello et al., 2018). However, how this translates to impacts on convective clouds and rainfall remains uncertain (Gentine et al., 2019).

The coupling between land surface properties and clouds involves simultaneous changes to the surface energy budget, and boundary layer moisture and temperature responses. At times, thermodynamic changes act in opposition: switching from a vegetated surface to bare ground leads to low-level warming and drying, which have opposite impacts on convection (C.-C. Chen et al., 2019). The net impact of these contrasting feedbacks appears to depend on the background meteorology (Findell & Eltahir, 2003) and cloud type (Baidya Roy & Avissar, 2002; Cioni & Hohenegger, 2017), both of which vary across the course of the day. Changes in clouds caused by land cover changes in turn drive shifts in the energy budget. Moreover, the surface energy budget itself changes over the day as the balance between radiation, turbulent fluxes, and surface heating is repartitioned in response to diurnal changes in insolation. These interactions between the surface and convection further complicate the cloud response to deforestation, particularly since this land-atmosphere coupling evolves on diurnal timescales.

Recent satellite-based estimates suggest deforestation in Southeast Asia locally enhances cloud cover (Xu et al., 2022; Leung et al., 2024), though the magnitude of the cloud response appears to depend on background meteorology and time of day. Although such observational quantifications are essential, it is challenging to extract information about the mechanisms driving cloud responses from these long-term estimates. This observational work must thus be complemented with process-oriented modeling studies.

Most modeling-based investigations of deforestation impacts over Southeast Asia have used global or regional climate models, which allow for long integration times to assess the climatic implications of these widespread changes in land cover (Werth & Avissar, 2005; Schneck & Mosbrugger, 2011; Takahashi et al., 2017; Tölle et al., 2017; C.-C. Chen et al., 2019; H.-C. Chen & Lo, 2023). However, disagreements remain about the sign of deforestation impacts on cloud cover. This is perhaps to be expected, given that processes driving convection (especially shallow clouds) are not explicitly resolved in large-scale models and are thus sensitive to how models parameterize convective responses to these compensating deforestation impacts on moisture and temperature (C.-C. Chen et al., 2019). This uncertainty highlights the need to improve our understanding of land surface-convection interactions at scales where convective processes can be more accurately resolved, especially in regions like Southeast Asia where most convection is driven by diurnally reversing mesoscale flows (e.g., sea breezes, terrain flows) that are sensitive to surface properties (Qian, 2008; Yang & Slingo, 2001).

Despite these challenges in quantifying cloud responses to forest loss, doing so is essential to fully characterizing deforestation impacts on weather, hydrology, and the Earth's energy balance (Pielke Sr., 2001; Boysen et al., 2020; Laguë et al., 2021). Such impacts may also vary between different types of convection (Gentine et al., 2019). Thus, we must understand how different cloud types and associated precipitation rates respond to changes in the land surface.

This research aims to quantify the impacts of deforestation on a range of tropical convection morphologies, as well as elucidate the physical mechanisms driving these impacts. Specifically, we address the following two science questions: (1) how does deforestation impact different cloud types across the diurnal cycle? and (2) what is the impact of those cloud responses on surface precipitation? We address these questions using cloud object-tracking techniques applied to a pair of high-resolution simulations with forested and deforested land cover, described in **Section 2**. We quantify how these land surface changes impact the surface energy budget and near-surface atmosphere in **Section 3**. In **Section 4**, we quantify impacts of the initiation of tracked cloud objects across the diurnal cycle. We discuss how these deforestation-driven shifts in the cloud distribution impact precipitation in **Section 5**. Finally, we summarize our findings and discuss broader implications of this work in **Section 6**.

2 Methods

2.1 Model description and configuration

We conducted large eddy simulations (LES) using the Regional Atmospheric Modeling System (RAMS version 6.3.04) (Pielke Sr. et al., 1992; Cotton et al., 2003; Saleeby & van den Heever, 2013). Full information about the model settings is provided in **Table 1**, but we describe key aspects of the simulation design and model set-up below.

Table 1. RAMS model parameters

Model aspect	**Description**
Grid	Arakawa-C grid
	2150 x 2230 points, $\Delta x = \Delta y = 150$m
	106 vertical levels, $\Delta z = 50\text{-}300$m with a stretch ratio of 1.04
Timestep	$\Delta t = 1.5$s
	Output every 5 minutes
Integration time	6 hours spin-up time (excluded from analysis) + 72 hours (3 diurnal cycles)
Initialization	Initialized from ERA-5 (Hersbach et al., 2020)
Boundary conditions	Nudged with hourly ERA-5 data at lateral (25 grid points from side) and top (above 22km) boundaries with nudging timescale = 900s (15 mins)
Surface scheme	Land Ecosystem-Atmosphere Feedback (LEAF-3) (Walko et al., 2000)
	Land cover taken from HILDA+ (Winkler et al., 2021) matched to LEAF-3 land cover classes
	Soil classes taken from UN FAO dataset (FAO United Nations, 1974)
	11 soil layers extending to 0.5m below the surface, with soil moisture and temperature initialized from ERA-5
Turbulence scheme	Smagorinsky (1963) with modifications from Lilly (1962) and Hill (1974)
Microphysics scheme	RAMS two-moment bin-emulating microphysics (Meyers et al., 1997; Saleeby & Cotton, 2008)
Radiation scheme	RTE-RRTMGP (Pincus et al., 2019)
	Radiation tendencies updated every 5 minutes
Aerosol treatment	Aerosol number concentration = 600 cm^{-3} at surface, exponentially decreasing with height with scale height of 7km
	Fixed aerosol concentrations (no sources, sinks, or advection)
	Aerosol-radiation interactions are represented

Our simulations are designed to reproduce the diurnal cycle of convection (**Figure 1**), including the daytime transition from shallow to deep convection during synoptically benign conditions, when convection is primarily driven by local thermodynamics rather than large-scale forcing. The simulation domain (**Figure 2**) encompasses a large area (~322x334km) in northwestern Borneo, around Kuching, Malaysia. This region experienced extensive land cover changes over the past few decades (**Section 2.2**). The morphology, timing, and distribution of clouds in our simulations are similar to observed cloud patterns (**Figure 1**). We note, however, that we analyze these simulations in a statistical manner to examine land-convection interactions in the region, rather than as a case study recreating specific meteorology from a specific day.

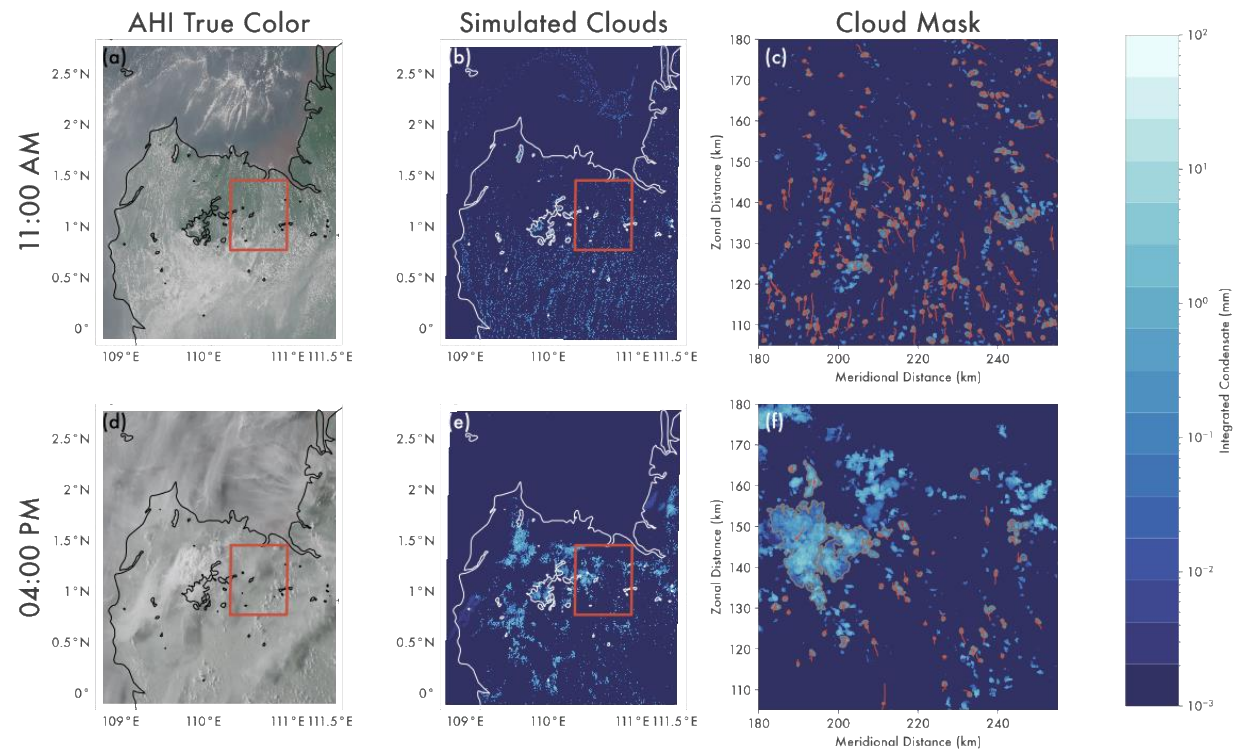

Figure 1. Simulations reproduce the observed diurnal cycle and distribution of convection, shown for 11:00a.m. (a-c) and 4:00p.m. (d-f) on 17 September 2019. Advanced Himawari Imager (AHI) true color imagery (left) compared to integrated condensate from the VEG2019 simulation (center). Black (a,d) and white (b,c,e,f) contours show coastline and 500m a.s.l. Red boxes (a,b,d,e) indicate the region in (c,f) used to demonstrate the *tobac* cloud identification approach, including cloud object centers (red circles), trajectories (red lines), and outlines of the cloud masks (gray contours).

To adequately resolve fine-scale atmospheric features driving the initiation and development of shallow cumuli, we used a fine spatiotemporal resolution ($\Delta x = \Delta y = 150$m, $\Delta z = 50$-300m, $\Delta t = 1.5$s). This, in combination with our large model domain integrated over three diurnal cycles (72 hours, 17-20 September 2019) allowed us to extensively sample the trimodal distribution of tropical convection (Johnson et al., 1999). Our simulation period was directly before the transition from southwest to northeast monsoon (Reid et al., 2023). We initialized and nudged the lateral boundary conditions using ERA-5 reanalysis (Hersbach et al., 2020), which constrained the synoptic scale environment while ensuring that convective and mesoscale features evolve freely in the domain.

Two-way land-atmosphere exchanges were parameterized using the Land Ecosystem Atmosphere Feedback (LEAF-3) (Walko et al., 2000) surface model. LEAF-3 represents turbulent and radiative exchange between the soil/ground, vegetation, and a canopy layer, which then exchanges energy, water, and momentum with the lowest atmospheric layer.

2.2 Experiment set-up

We conducted two simulations constrained with the same atmospheric initial boundary conditions but different land cover. Using identical large-scale atmospheric forcing allowed us to compare how land-atmosphere interactions impact local convective development.

Land cover was taken from the Historic Land Dynamics Assessment+ (HILDA+) dataset (Winkler et al., 2021), which combines remote sensing and long-term statistical datasets to estimate land cover (Δx,y=1km) from 1960-2019. HILDA+ land cover classes do not directly correspond to those in LEAF-3. Thus, we adapted HILDA+ land cover for use in our simulatiosn by identifing which HILDA+ categories most closely matched the observed spatial patterns in

2019 land cover from MODIS (Friedl et al., 2002) and the default RAMS land cover. Land surface properties key to this study used in the numerical experiments are shown in **Figure 2**.

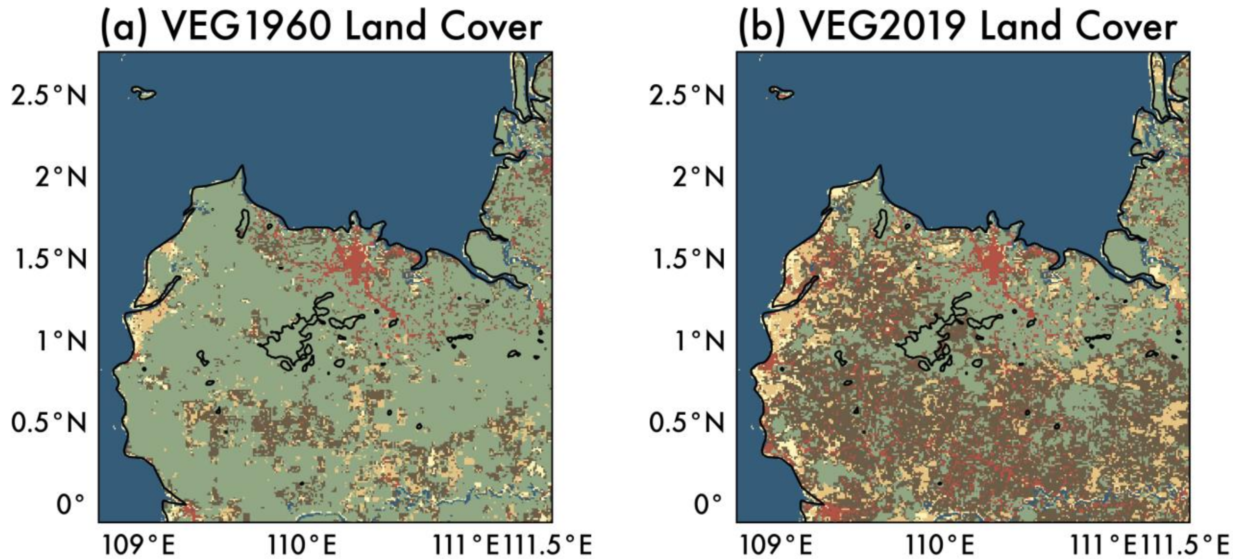

Land Cover Type	Vegetation Height (m)	Albedo	Min. Evaporative Resistance (s m^{-1})
Ocean	-	-	-
Evergreen broadleaf forest	32	0.15	500
Wooded grassland	7	0.18	100
Crop/mixed farming	1	0.18	100
Short grass	0.3	0.26	100
Urban	6	0.18	500

Figure 2. Model land cover set-up for (a) VEG1960 and (b) VEG2019. Black contours show coastline and 500m a.s.l. topography. Legend shows land surface properties in LEAF-3 relevant to this study.

We ran one simulation with land cover from 1960 (VEG1960) and one with land cover from 2019 (VEG2019) (**Figure 2**). By using a realistic distribution of land cover rather than total deforestation (Werth & Avissar, 2005; Takahashi et al., 2017) or an idealized checkerboard-type pattern (Rieck et al., 2014), we can examine the effects of realistic scales of deforestation and patterns of landscape heterogeneity.

The primary land cover change between 1960 and 2019 is a widespread shift from “evergreen broadleaf forest” representing intact tropical rainforests to “wooded grassland” and “cropland” representing plantations of oil palm, rubber, and other agricultural uses. Increases in “urban surface” are also evident. We refer to these three predominant non-forest land cover types as “deforested”. Compared to intact rainforests, deforested land has a lower surface roughness /

shorter canopy height and larger albedos (**Figure 2**). Deforested areas also have lower evaporative resistance, since forest vegetation retains more water for a given temperature increase.

It is important to note that unlike other modeling studies examining deforestation in Southeast Asia that replace forest with C4-type grass (Tölle et al., 2017; C.-C. Chen et al., 2019), forest is primarily replaced by "wooded grassland" in our simulations. This surface type best matches observations of oil palm and rubber plantations in terms of land surface properties including vegetation height (June et al., 2018) and evaporative resistance (Giambelluca et al., 2016). In contrast to regions like the Amazon where deforestation is primarily driven by conversion to cropland or pastureland, transitions from tropical forest to palm oil and rubber plantations in Southeast Asisa are unique in that they do not necessarily reduce evapotranspiration (Spracklen et al., 2018).

2.3 Cloud object identification and tracking

We tracked convective clouds across their lifecycles using the Tracking and Object Based Analysis of Clouds (*tobac* version 1.5) algorithm (Heikenfeld et al., 2019; Sokolowsky and Freeman et al., 2024). Below is a brief description of how we used *tobac.* We direct readers to the cited papers for details of the *tobac* algorithm.

First, we identified updrafts as contiguous three-dimensional regions with local vertical velocity maxima >1 m s^{-1} (with additional thresholds every 2 m s^{-1} between 2 and 50 m s^{-1} to separate updrafts of varying intensities) and volume >64 grid points (0.072-0.432 km^3, depending on vertical location) depending on vertical location). Second, we connected updrafts temporally by linking their projected trajectories in time. Any updrafts with lifetimes <15 minutes were excluded from our analysis to ensure we only analyze clouds that are well-captured across their life cycle. Third, we used watershedding to identify contiguous regions around each updraft that have vertical velocities >1 m s^{-1} and cloud condensate mixing ratios >0.01 g kg^{-1}. Regions with collocated updraft and condensate are considered "clouds". Thus, we separate cloudy updrafts from dry boundary layer thermals. Finally, we calculated key properties for each cloud object, including cloud lifetime, cloud base height (CBH), cloud top height (CTH), CTH growth rate, and mean precipitation rates.

The large dataset of identified clouds (>75,000 per simulation) allows for robust statistical assessment of a range of cloud modes, each of which may be coupled to the land surface via different processes. We required that all clouds initiate from within the boundary layer (with their updraft centroid at the time of first detection <2.5km). We excluded high clouds originating offshore or outside our domain from our analysis. While high cirrus is ubiquitous in the region, the origin of such clouds offshore or outside our domain are not directly impacted by the surface perturbations we test here. The specific thresholds utilized here are ultimately subjective, but testing of these parameters showed qualitatively similar results. *tobac*-tracked cells account for >80% of the total surface precipitation in the domain, adding confidence that our methods capture most of the convective clouds of interest to our science questions. Examples of cloud masks and tracks generated using *tobac* are shown in **Figure 1c,f**.

3 Deforestation impacts on the surface energy budget

We begin by examining the surface energy budget, diurnally averaged over land (**Figure 3**). It is important to note that we use a sign convention of negative values indicating terms which cool the surface (energy transferred from surface to atmosphere or ground). The magnitude of radiative and turbulent heat fluxes in our simulations compare favorably with flux measurements over rainforests and oil palm plantations in Borneo (Fowler et al., 2011; Takanashi et al., 2010; Tang et al., 2019). The magnitude of latent heat fluxes (LHF) is larger than that of sensible heat fluxes (SHF), due to the abundant moisture in the soil and vegetation canopy. Prior to the onset of clouds, the mean Bowen ratio (B=SHF/LHF) ranges from 0.3-0.5 between 7-9a.m. (here and throughout the text, times are local time, i.e., UTC+8).

Deforestation from VEG1960 to VEG2019 (solid versus dashed lines; **Figure 3a**) drives robust shifts in the surface energy budget (**Figure 3b**). Positive changes in **Figure 3b** indicate deforestation leads to more energy transfer *into* the surface (or less transfer *out* of the surface). Similar trends are evident across all simulation days.

Changes to the surface energy budget between the two simulations are dominated by SHF impacts (red lines; **Figure 3**). Deforestation reduces energy transfer from the surface to the atmosphere via SHF (a decrease in SHF magnitude). This is driven by the reduced surface roughness associated with changes from tall rainforest to shorter palm oil plantations. The smoother deforested surface in the latter is less efficient at transmitting energy into the atmosphere through turbulent fluxes.

As a result of the less efficient turbulent exchange in the deforested regions, more energy accumulates at the surface and is used in heating the vegetation canopy and the ground (gray lines; **Figure 3**). We confirm this by examining vegetation canopy and near-surface (~25m a.g.l.) air in **Figure 4**. Indeed, the increased energy storage results in warmer land surface temperatures and warmer air at canopy level throughout the day (**Figure 4c**), consistent with satellite-based observations (Sabajo et al., 2017; Crompton et al., 2021) and field measurements (Hardwick et al., 2015). However, this energy is not efficiently transmitted from the smooth surface into the atmosphere, resulting in a more modulated near-surface temperature diurnal cycle in VEG2019 compared VEG1960 (**Figure 3b**). Rather than transferring energy through turbulent fluxes, the smooth deforested surface radiates more energy as outgoing longwave radiation (OLR) (green lines; **Figure 3c**).

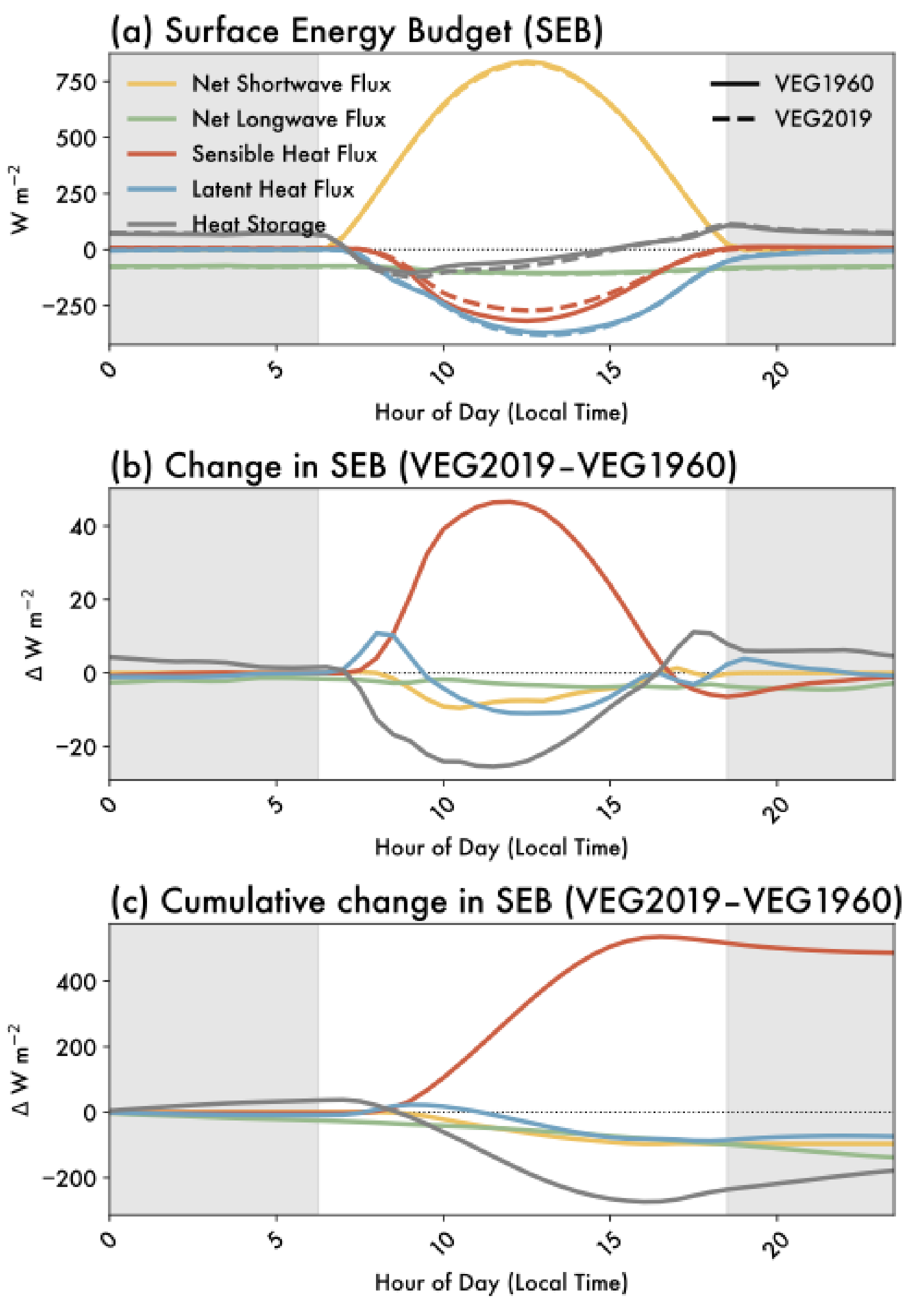

Figure 3. Diurnal evolution of the surface energy budget. (a) Mean surface energy budget, where positive terms heat the surface and negative terms cool the surface. Solid lines are VEG1960, and dashed lines are VEG2019. Differences between VEG2019 and VEG1960 are shown as (b) instantaneous and (c) cumulative changes. Gray shading shows nighttime hours.

The warmer canopy air in VEG2019 enhances evapotranspiration (ET), with most of the energy stored in the canopy going into latent heating. The deforested areas have lower evaporative resistance, meaning for a given temperature, they release more moisture into the atmosphere than forested regions. Deforestation thus moistens canopy air (**Figure 4c**). LHF, like SHF, depends on the efficiency of turbulent surface-atmosphere exchange and is hampered by the smoother deforested surface. However, since there is a larger moisture source due to enhanced ET, LHF is enhanced in the deforested scenario after 9a.m. (blue lines; **Figure 3**) once the canopy heats up sufficiently for ET to counteract reduced turbulence. This response reflects deforestation in moist, tropical environments where forests are primarily converted to oil palms or other agricultural lands that retain high soil moisture (van der Molen et al., 2006)—if deforestation instead converted the forested area to bare soil (or moisture-limited vegetation) LHF would likely differ (C.-C. Chen et al., 2019; Drager et al., 2020; H.-C. Chen & Lo, 2023).

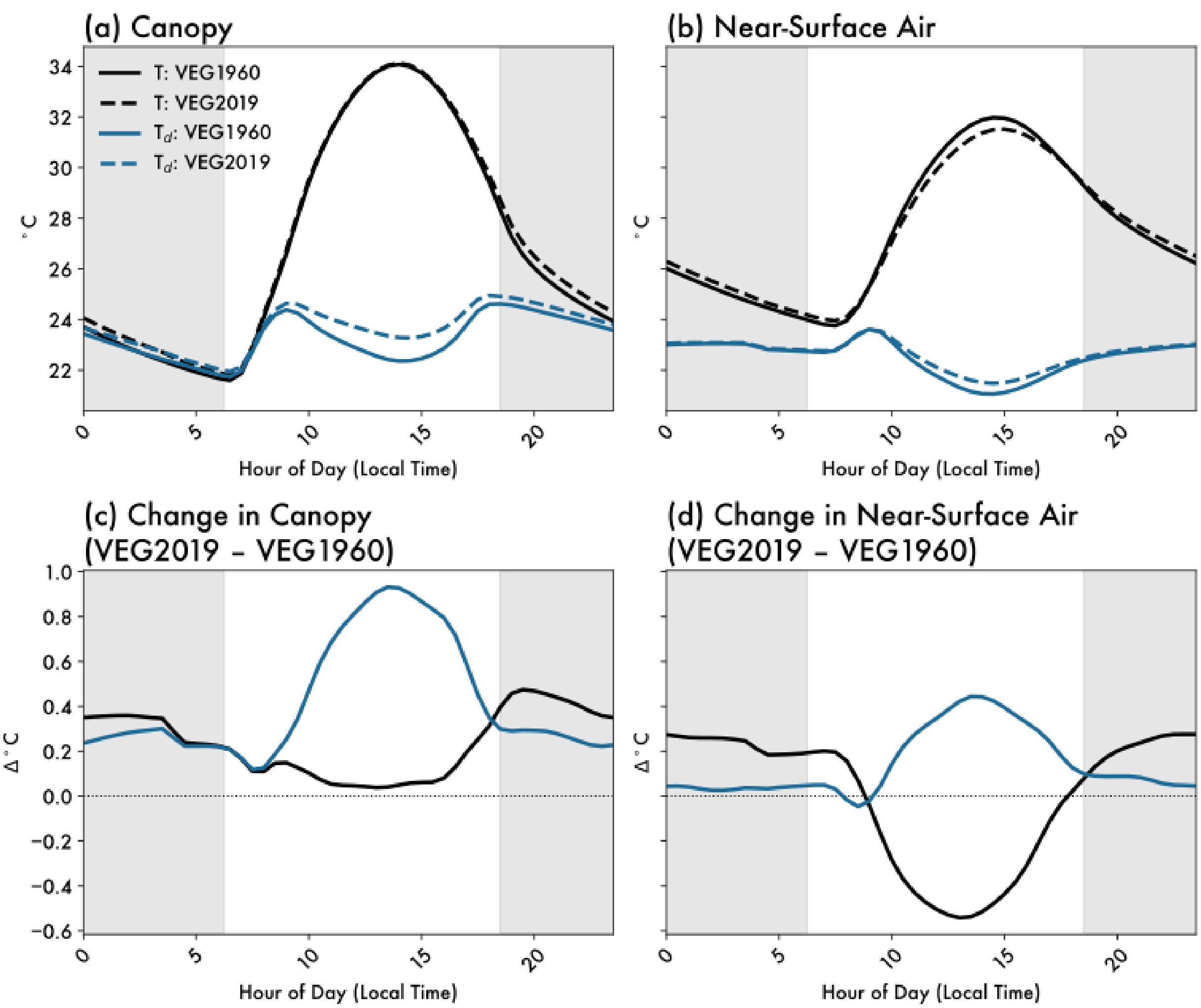

Figure 4. Diurnal evolution of air in (a) the vegetation canopy and (b) at the lowest near-surface atmospheric level for temperature (black) and dewpoint (blue). Solid lines are VEG1960, and dashed lines are VEG2019. Differences between VEG2019 and VEG1960 are shown for (c) canopy and (d) near-surface air. Gray shading shows nighttime hours.

Changes in the surface energy budget following deforestation are dominated by non-radiative properties (surface roughness and evaporative resistance) rather than radiative properties (albedo) (**Figure 3**), which is consistent with past research for the tropics (Davin & de Noblet-Ducoudré, 2010; Duveiller et al., 2021). We observe <1% decrease in the magnitude of early morning (7-9a.m.) net shortwave (SW) flux following deforestation due to the more reflective surface. Once clouds develop after 9a.m., there is a bigger deforestation impact on SW (yellow line; **Figure 3**). However, changes due to reduced cloud cover (more downwelling SW) and increased albedo (more upwelling SW) act in opposite directions, such that the SW contribution to surface energy budget changes is secondary compared to changes in SHF.

4 Cloud responses to deforestation

4.1 Overview of cloud evolution

Our simulations capture the trimodal convection distribution (Johnson et al., 1999) and shallow to deep convection transition in the Maritime Continent (Renggono et al., 2001; Argüeso et al., 2020; Marzuki et al., 2022). **Figure 5** demonstrates the mean distribution of cloud number and area binned by CTH across the diurnal cycle. We show mean cloud development (white arrows; **Figure 5a,b**), calculated as the mean change in CTH over five-minute intervals for all cells within a given bin.

The surface heats up after sunrise (6:15a.m.) until shallow cumulus develop around 9a.m. These shallow cumuli (1km<CTH<3km) are mostly non-precipitating and organize in cloud streets. By 12p.m., the sea breeze has propagated onshore, and congestus (4km<CTH<10km) have formed along the convergence zone ahead of the sea breeze. These convective cells precipitate more strongly than cells that develop earlier in the day, and produce cold pools that collide, creating areas of low-level convergence. Some collisions result in deeper cumulonimbus (CTH>10km) from 4–6:30p.m., while other less favorably located congestus only reach maximum CTHs of ~8km before dissipating. This division between congestus which eventually become deep convection (transient congestus) and those which do not (terminal congestus) (Luo et al., 2009; Leung & van den Heever, 2022) is evident as the bifurcation in the mean cloud development (white arrows; **Figure 5a,b**).

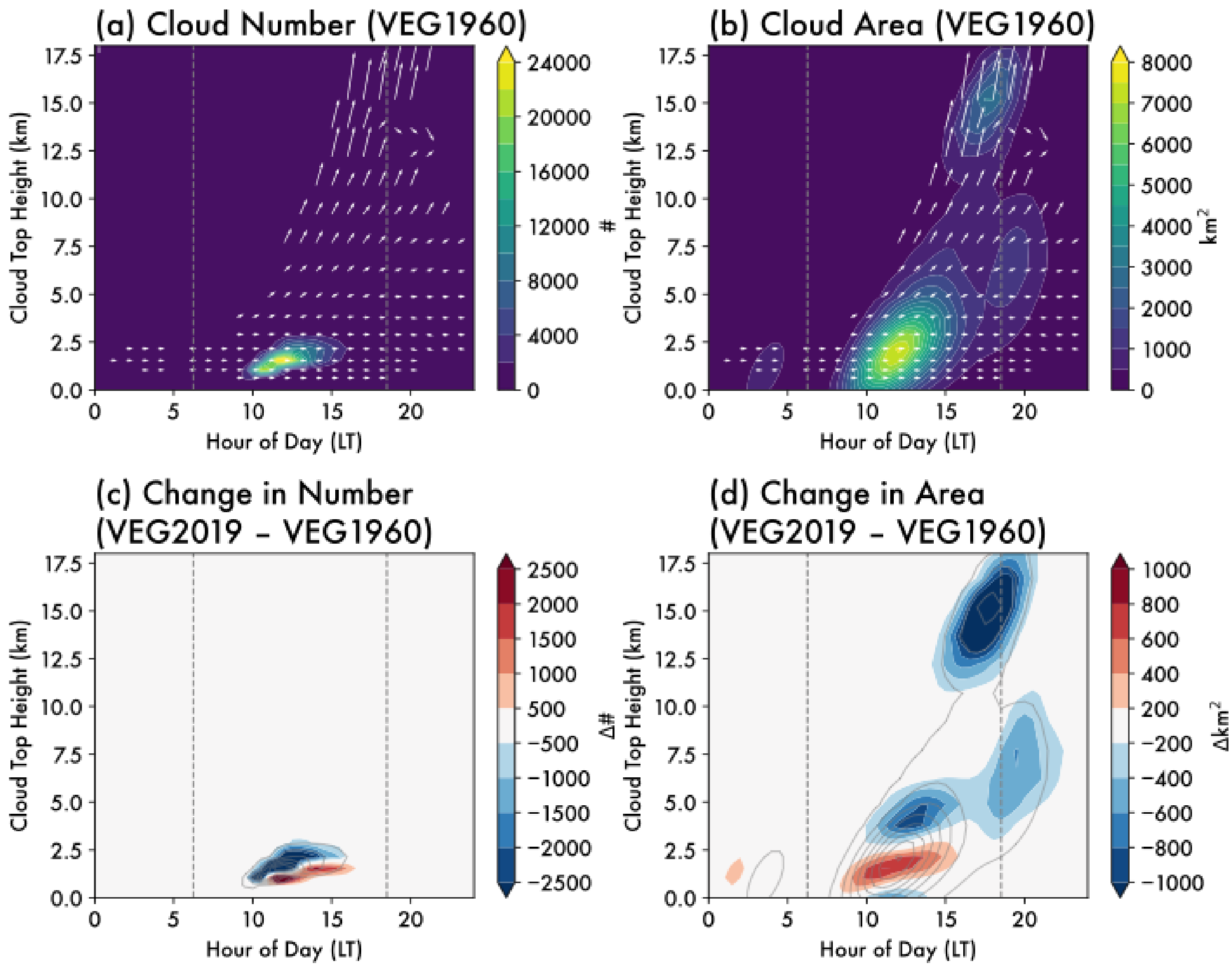

Figure 5. Diurnal cycle of total cloud number and area. Color contours show total (a) number and (b) area of *tobac*-tracked clouds for each joint hour of day and cloud top height (CTH) bin in VEG1960. Height of arrows indicate the mean change in CTH for a given (hour of day, CTH) bin, while the length of arrows is uniform and arbitrary. Difference between VEG2019 and VEG1960 is shown for cloud (c) number and (d) area, with gray contours from (a,b) for comparison. Gray vertical lines indicate sunrise and sunset.

4.2 Mean shallow cloud response

Deforestation-driven changes in surface-atmosphere interactions manifest as shifts in the cloud distribution (**Figure 5c,d**). Due to weaker SHFs (**Figure 3**), there are fewer dry boundary layer thermals, and the planetary boundary layer (PBL) deepens more slowly in VEG2019 than in VEG1960. The lifted condensation level (LCL) is lower following deforestation (**Figure 6a,c**), meaning parcels lifted from the surface should form clouds at lower altitudes. However, the weakened SHFs limit the ability of thermals to penetrate the LCL and form clouds.

Deforestation thus shifts the peak in the cloud diurnal cycle to later in the day, once the PBL is sufficiently developed.

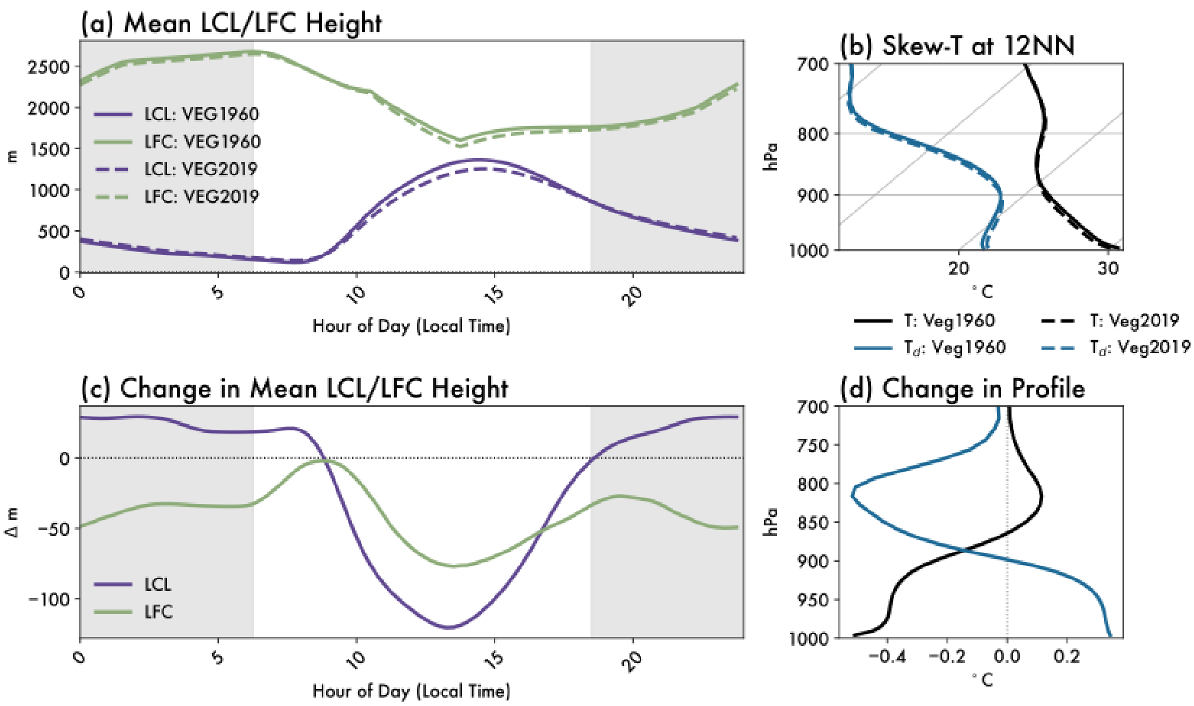

Figure 6. Diurnal evolution of lifted condensation level (LCL) and level of free convection (LFC). (a) LCL height in purple and LFC height in green. (b) mean skew-T profile at 12p.m., with temperature (black) and dewpoint (blue). Solid lines are VEG1960, and dashed lines are VEG2019. Differences between VEG2019 and VEG1960 are shown for (c) LCL/LFC evolution and (d) atmospheric profile. Gray shading (a,c) shows nighttime hours.

The cloud response to lower SHFs following deforestation is counteracted by increased LHFs and evapotranspiration (**Figure 3**). Although the near-surface atmosphere is moister in the deforested scenario (**Figure 6b,d**), this moisture is not transported vertically given the limited turbulent mixing over smoother deforested surfaces. The lower LCL in VEG2019 coincides with an increased distance between the LCL and the level of free convection (LFC) around midday, meaning enhanced convective inhibition (**Figure 6a,c**). Even if parcels reach the LCL more easily in VEG2019, they are not positively buoyant and less likely to become active shallow cumuli (Stull, 1988; Gentine et al., 2013).

4.3 The role of mesoscale circulations

Mesoscale circulations locally impact cloud frequency in **Figure 7**, which shows the deforestation-driven change in amplitude of the diurnal cycle of cloud initiation. We calculate the mean cloud diurnal cycle based on the number of clouds occurring in each 6x6km box at each time of day (15-minute increments). We tested other averaging windows in space (1.5–15km) and time (5–60 minutes), and found the results were qualitatively similar; we select these parameters for clarity of visualization. For each location, we find the diurnal peak in the number of clouds and compare this peak for VEG2019 and VEG1960. **Figure 7** thus accounts for temporal offsets in the diurnal cycle (e.g., if cloud development peaks later / earlier in the day). For most regions, there is a decrease in peak cloud number, consistent with our earlier findings that deforestation suppresses shallow cumuli (**Figure 5c**). However, there are some areas where cloudiness is enhanced following deforestation (red points; **Figure 7a**). In these regions, cloud number and cloud fraction are greater at midday following deforestation (**Figure 7c,e**).

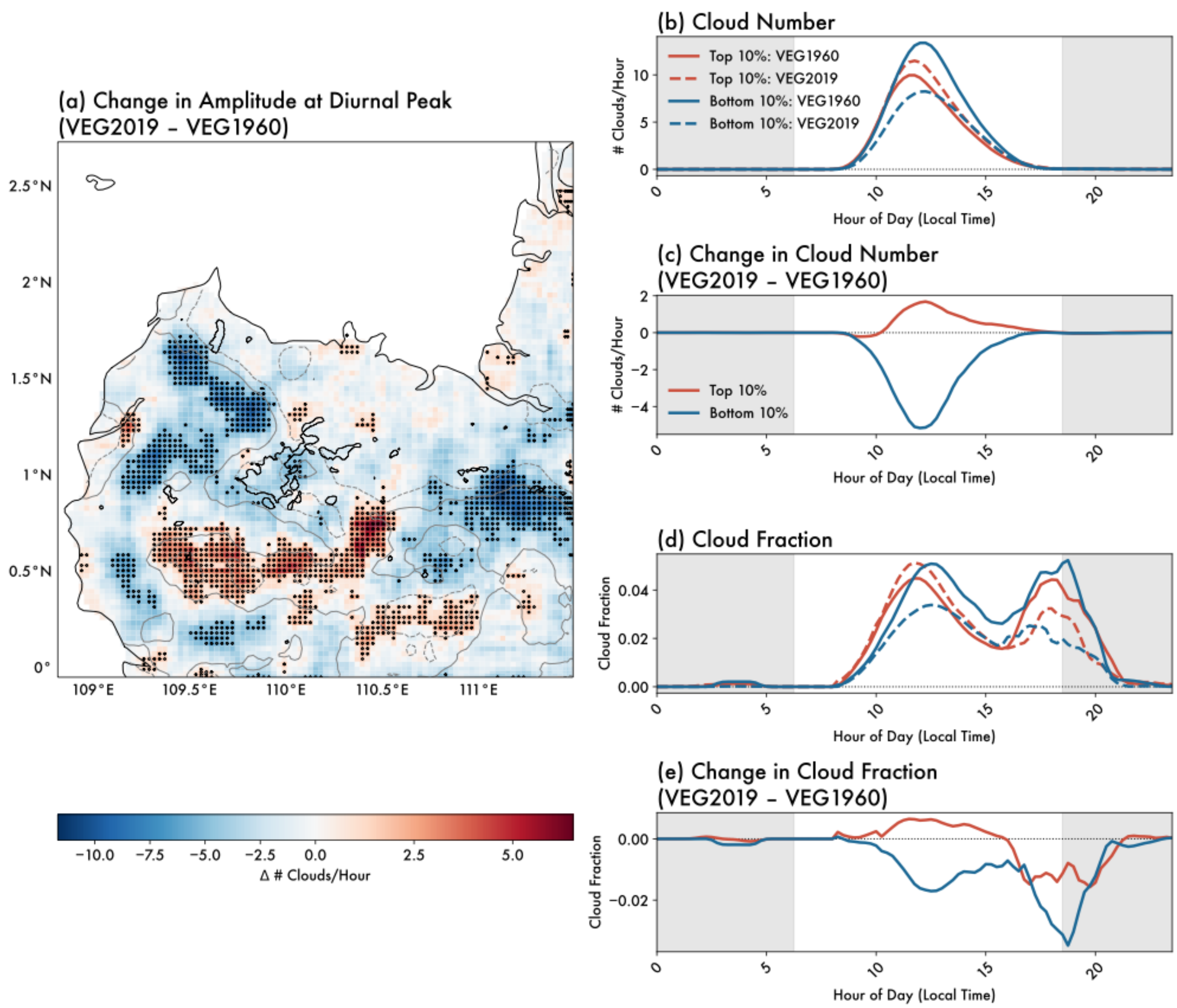

Figure 7. Spatial heterogeneity in cloud response to deforestation. (a) Difference in the amplitude of the diurnal peak in cloud formation between VEG2019 and VEG1960, as described in text. Gray contours show 25% (dashed) and 50% (solid) forest loss between VEG1960 and VEG2019. Black contours show coastline and 500m a.s.l. Circles represent top (red) and bottom (blue) decile of points in terms of the change in the cloud diurnal peak, used for averaging in (b-e). Mean diurnal cycle of cloud (b) number and (d) fraction are shown for the top / bottom decile of points, with the VEG1960 simulation in solid lines and VEG2019 simulation in dashed lines. Changes are shown as the difference between VEG2019 and VEG1960 for cloud (c) number and (d) fraction. Gray shading (b-e) shows nighttime hours.

The spatial pattern of deforestation-induced cloud changes comprises dipole structures of cloudiness aligned along regions of forest loss from VEG1960 to VEG2019. Regions where cloudiness is enhanced tend to be located on the side of the deforestation boundary with less forest loss, suggesting the influence of mesoscale solenoidal circulations. **Figure 8** shows that regions of enhanced cloudiness coincide with areas where turbulent heat fluxes and near-surface virtual potential temperature are enhanced relative to area means. Local enhancements in cloudiness along the interface between pristine and perturbed land cover regions are driven by the ascending branch of these circulations on the warmer, drier side of the gradient. These mesoscale circulations—referred to as vegetation breezes (Saad et al., 2010; Khanna et al., 2017; J. Chen et al., 2023)—transport low-level moist air from more deforested regions (where LHFs are higher) to less deforested regions where air is positively buoyant and the circulations provide the lift for cloud formation. This results in local increases in forced cumuli around the deforestation boundary (Ascher et al., 2025; Falk et al., 2025).

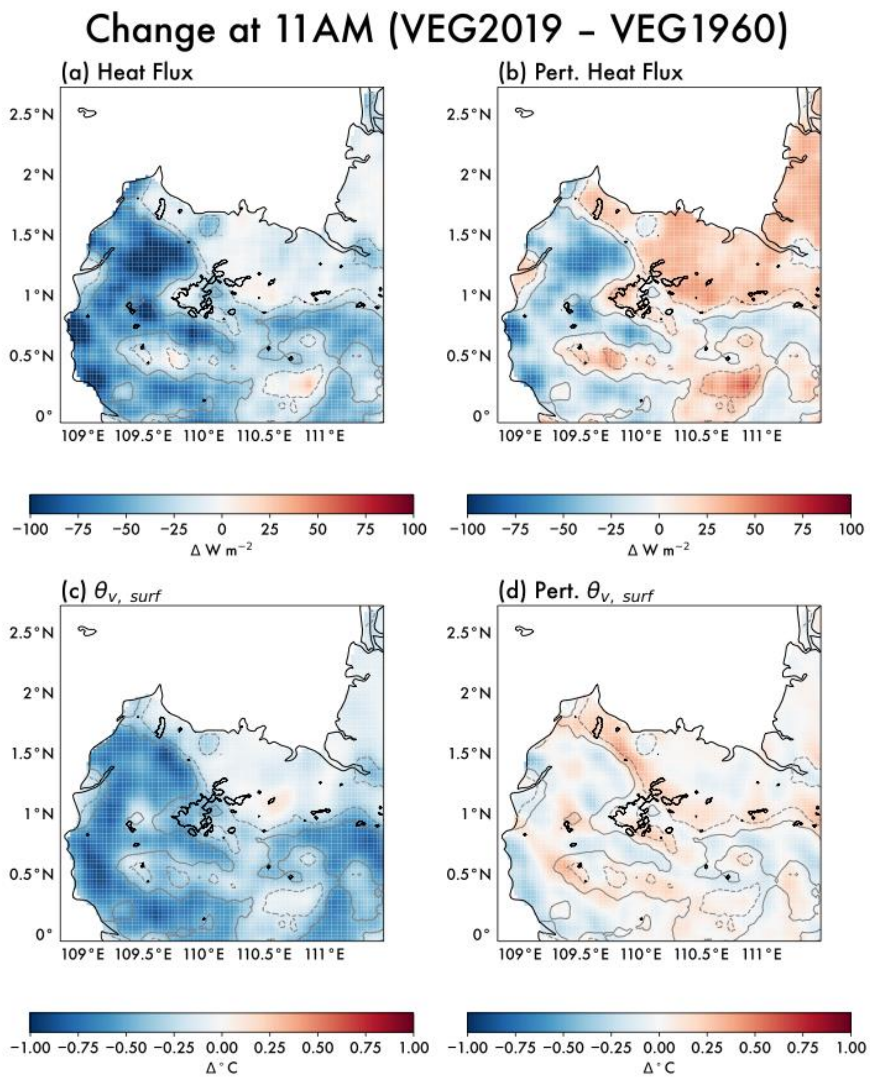

Figure 8. Mesoscale solenoidal circulations are driven by gradients in surface heat flux and buoyancy. Maps of (a) mean turbulent heat flux (sensible + latent) and (b) perturbation heat flux (perturbation from spatiotemporal mean for given hour) from 10:30-11:30a.m., prior to the peak in daytime convection. (c) and (d) show the same for the near surface virtual potential temperature. Gray contours show 25% (dashed) and 50% (solid) forest loss between VEG1960

and VEG2019. Black contours show coastline and 500m a.s.l. Data are aggregated to 3x3km, then smoothed with a 21x21km rolling window.

4.3 Impacts on sea breeze and deep convection

Across the domain, there is a reduction in deep convection following deforestation (**Figure 5b,d**). In part, this follows from reduced shallow cumuli earlier in the day (**Section 4.1**). Even once the decrease in midday shallow cumuli is accounted for, we still observe a further decrease in the proportion of clouds that develop into deep convection after deforestation. Taking the relative proportion of cloudy area between 4p.m. and 8p.m. (the peak of deep convective activity), 10% more cloudy area in VEG2019 is associated with terminal congestus when compared to VEG1960. These differences are due to differences in the large-scale moisture convergence associated with changes in the sea breeze.

The SSTs in the simulations are nearly identical. However, there is a near-surface cooling over land in VEG2019, which leads to a weakening of the sea breeze compared to VEG1960. **Figure 9** shows the diurnal average of low-level moisture flux convergence (MFC; vertically integrated from the surface to 1km a.s.l) as a function of distance from the coastline. The sea breeze does not penetrate as far inland (~2km closer to the coastline) and generally fluxes less moisture inland (maximum MFC is ~1 kg m^{-2} hr^{-1} lower) following deforestation. This is consistent with past research on surface roughness and evapotranspiration impacts on sea breeze strength and propagation (Gero & Pitman, 2006; Grant & van den Heever, 2014).

As a result of the reduced onshore moisture flux following deforestation, fewer deep convective cells initiate in the late afternoon (**Figure 5d**) along the sea breeze front (black contours; **Figure 9a,b**) in VEG2019 compared to VEG1960. Also, the development of the fewer deep convective clouds in VEG2019 is shifted to later in the evening (**Figure 7c**).

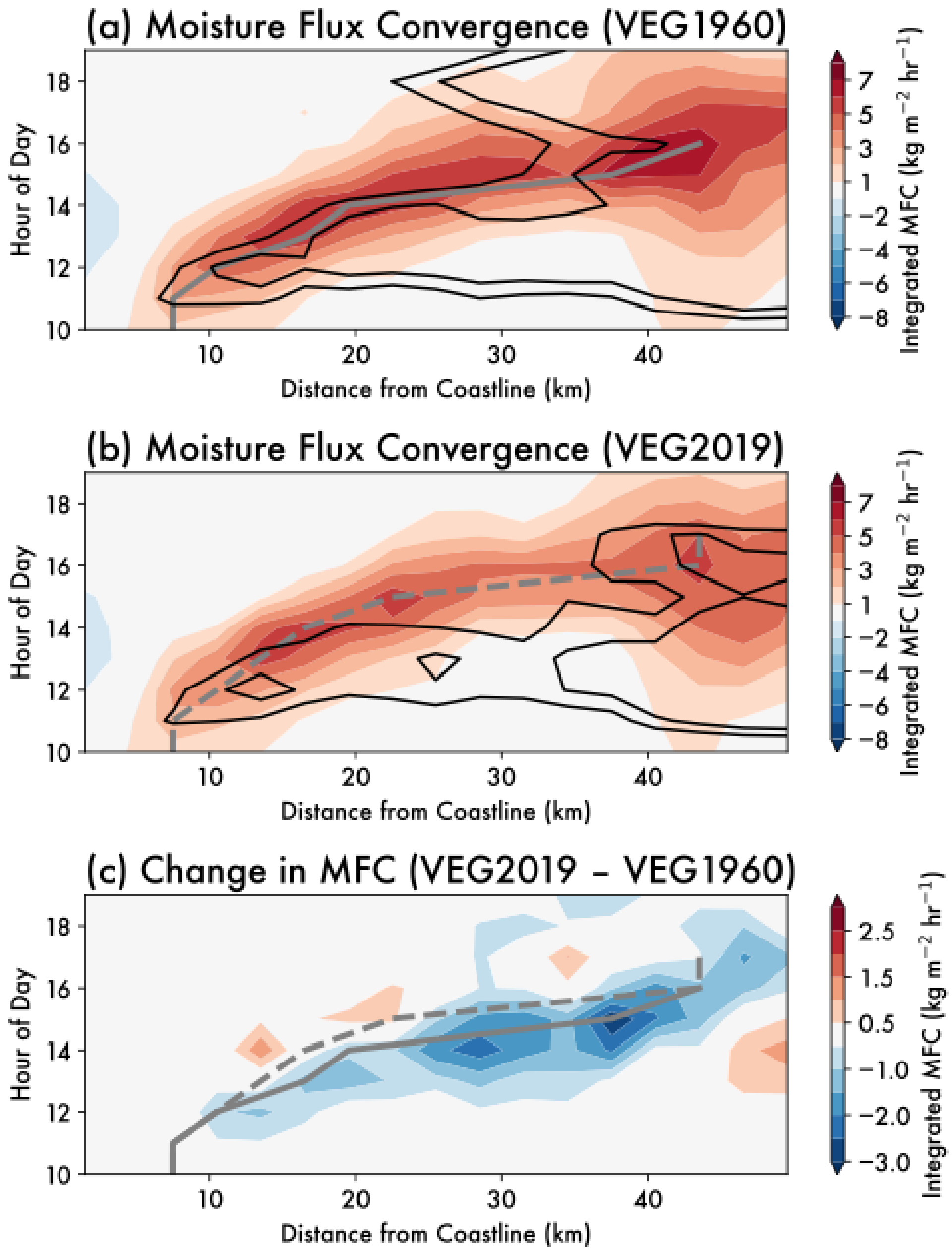

Figure 9. Hovmöller plot showing sea breeze propagation and associated moisture flux convergence (MFC) and cloud cover for (a) VEG1960, (b) VEG2019, and (c) the difference between VEG2019 and VEG1960**.** Color shading in (a) and (b) shows integrated MFC (surface–1km a.g.l.), as a function of distance from the coastline and hour of the day. Black contours show a cloud fraction of 3% and 3.5%. Gray lines show the location of peak MFC for each time in VEG1960 (solid) and VEG2019 (dashed).

5 Implications for precipitation

The changes to convection across the diurnal cycle caused by widespread deforestation have substantial implications for precipitation at the surface. **Figure 10** shows changes in the diurnal cycle of clouds across the domain, as in **Figure 7**, but only for clouds with appreciable rainfall at the surface (rain rate > 0.01mm hr^{-1}). The area with positive changes (i.e., more raining clouds) is more evenly distributed across **Figure 10a** compared to **Figure 7a**. Although mesoscale circulations support increased convection along the deforestation boundary, the change in *raining* cumuli is more spatially uniform. This suggests the increase in shallow cumulus rainfall is driven by domain-wide changes in low-level moisture rather than lifting driven by surface heterogeneities, though these may still play a secondary role. Fewer active shallow cumuli form in VEG2019, but those which do have access to more near-surface moisture and trigger the onset of precipitation earlier in the day (**Figure 10b,c** and **Figure 11a,c**). Although these precipitating shallow cumuli comprise a small number and a limited integrated contribution to the overall water budget, these deforestation-driven changes happen during a time of day when little precipitation generally occurs. Thus, any shifts have a large relative contribution to when and where rainfall occurs (8% increase in raining area and 20% increase in rain amount from shallow cumuli between 9a.m.–3p.m.).

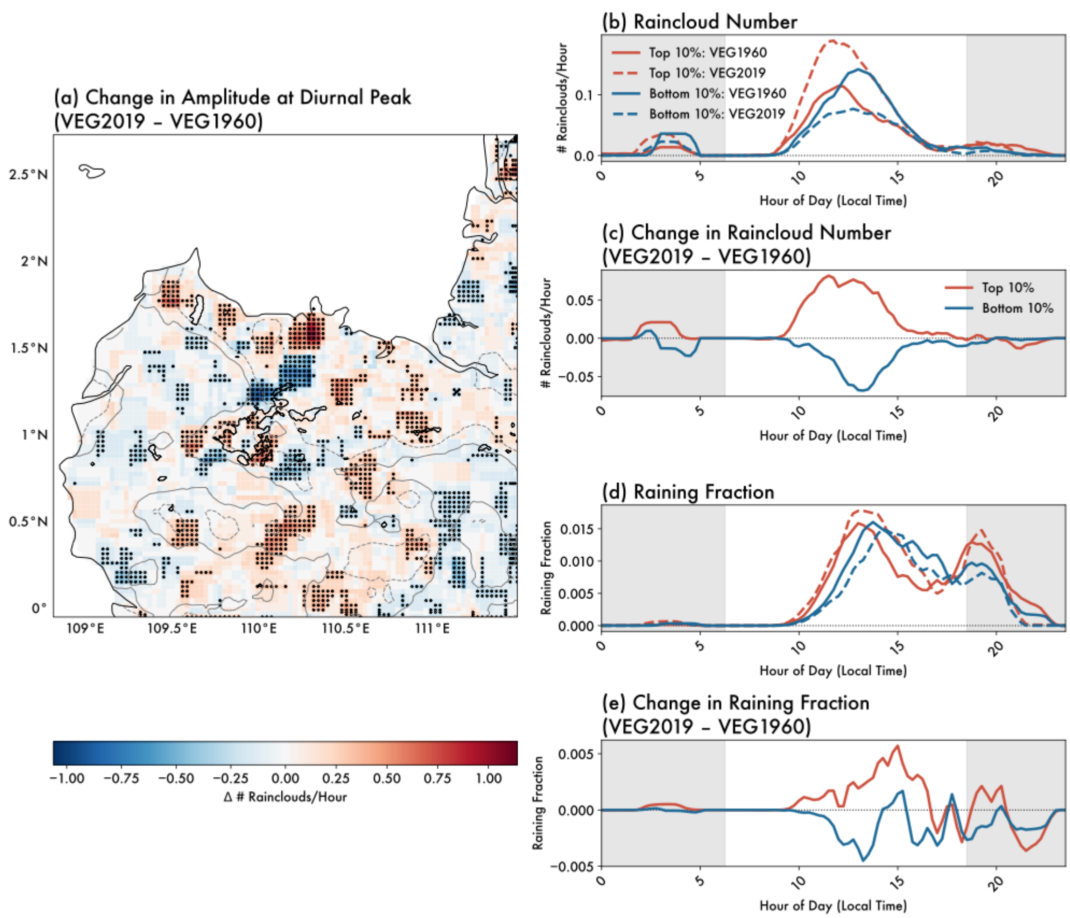

Figure 10. Spatial heterogeneity in raining cloud response to deforestation. As in **Figure 7**, but only for precipitating clouds (rain rate>0.01 mm hr^{-1}).

In contrast to the aforementioned changes in rainfall from shallow cumulus, we find that deforestation suppresses deep convection associated with sea breeze convergence, thereby leading to a decrease in the magnitude of the diurnal rainfall peak (**Figure 11d**). A majority of rainfall is driven by deep convection that forms after 3 p.m. (**Figure 11b**), and thus the net deforestation impact is a decrease in overall precipitation.

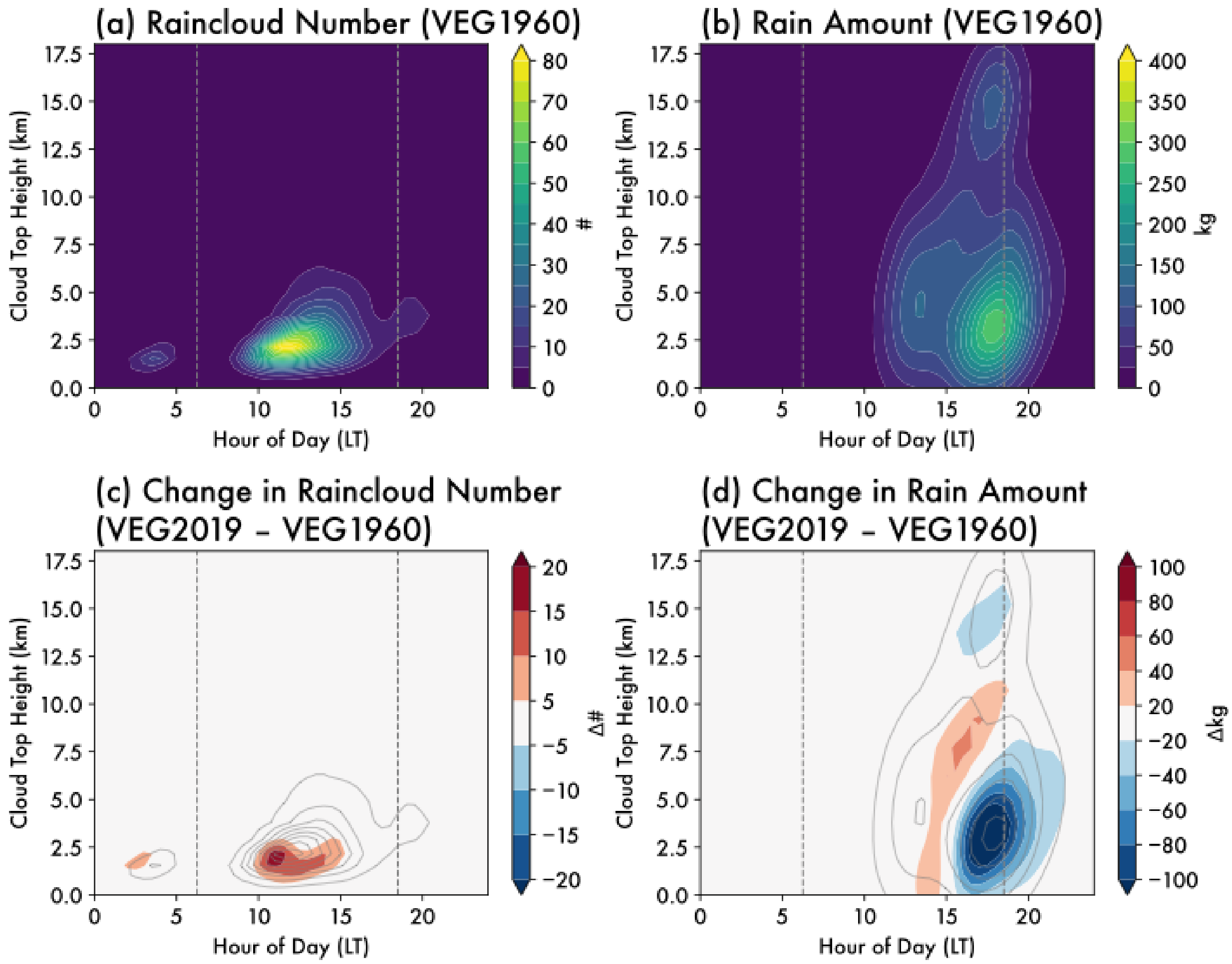

Figure 11. Diurnal cycle of (a) number of raining clouds and (b) total rain amount. As in **Figure 5**, but only for precipitating clouds (rain rate>0.01 mm hr^{-1}). Total rain amount (b,d) is integrated over cloud area.

6 Conclusions

Accelerating deforestation in many regions of the world, including Southeast Asia, motivates an urgent need to understand what impact such land cover changes have on clouds and precipitation. Global and regional climate models disagree about the sign of deforestation-induced cloud feedbacks, which demonstrates a gap in our understanding of the convective and mesoscale processes involved. In this study, we use a set of high-resolution large eddy simulations with varied land cover but identical atmospheric initial and boundary conditions to elucidate the mechanisms by which deforestation impacts clouds over Borneo. We focus on how land surface-convection interactions are influenced by changes to mean thermodynamics and mesoscale features like vegetation breezes and sea breezes. **Figure 12** illustrates the major processes governing these interactions.

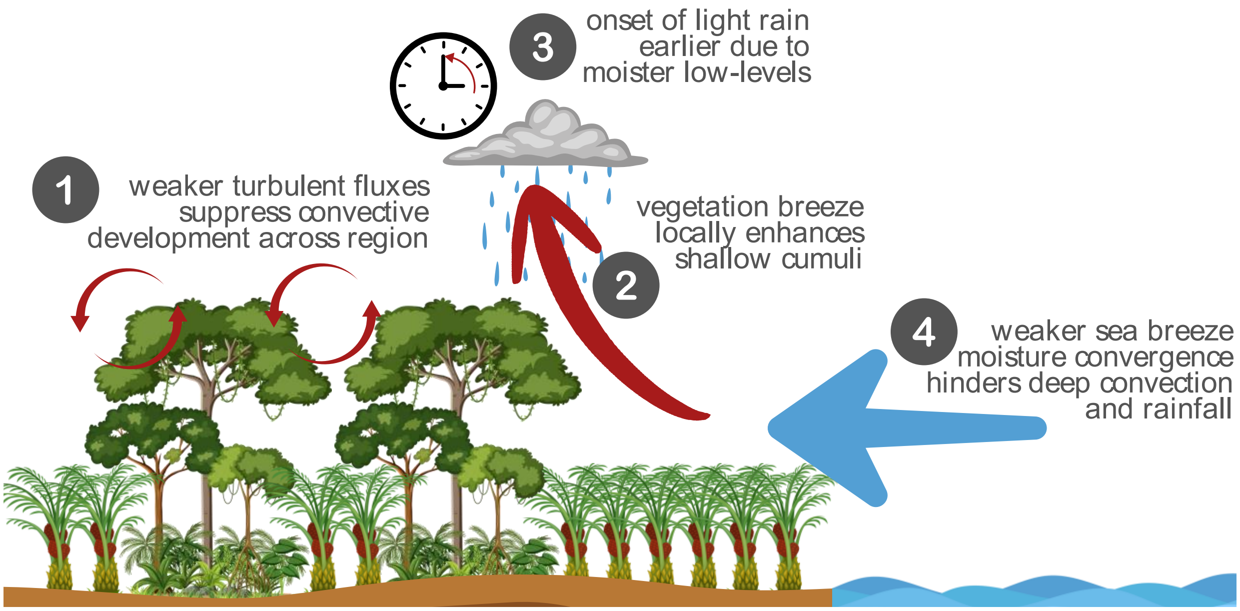

Figure 12. Schematic of major processes impacting the cloud response to deforestation over Borneo. As intact tropical rainforest is replaced by palm oil plantations, turbulent exchanges between the land and atmosphere are reduced across the region, which suppresses convective development overall (1). However, along the border of deforested areas, vegetation breezes can locally enhance midday shallow cumuli (2). Due to the moister low-level atmosphere, shallow cumuli which do form after deforestation tend to rain earlier in the day (3). The large-scale changes to the near-surface atmosphere over land weaken moisture flux convergence by the sea breeze, which hinders the development of deep convection in the evening (4).

Overall, we find deforestation induces robust changes to the surface energy budget and thermodynamic responses in the near-surface atmosphere. The shift from rainforest to palm and rubber plantations reduces surface roughness and makes turbulent land-atmosphere exchanges less efficient. This leads to a decrease in sensible heat fluxes that is primarily compensated for by a warming of the ground and vegetation canopy. Unlike in other tropical forest regions, where the conversion of forest to pasture or bare soil decreases latent heat fluxes, we find that under these moisture-rich conditions deforestation enhances evapotranspiration due to warmer canopies and weaker evaporative resistance. This unique surface response is consistent with observations (Fowler et al., 2011; Giambelluca et al., 2016; Spracklen et al., 2018), but has typically been neglected in climate modeling studies for this region (Takahashi et al., 2017; Tölle et al., 2017; C.-C. Chen et al., 2019). These changes to the surface energy budget lead to a cooler and moister near-surface atmosphere, and increases in convective inhibition following widespread deforestation, thereby changing the thermodynamic environment convection develops in.

Despite these clear energetic shifts, we find deforestation impacts on clouds are not homogeneous: changes to convection vary spatially and diurnally. Deforestation drives a decrease in late morning shallow cloudiness across the region via reduced sensible heat fluxes and enhanced convective inhibition. Yet we find shallow cloudiness is locally enhanced by vegetation breezes around areas with substantial forest loss. Local and regional deforestation impacts can therefore be in opposition. Quantifying the net deforestation impact on shallow clouds—which have strong radiative implications for climate (Gentine et al., 2019)—may depend on how extensive these vegetation-driven mesoscale circulations are, and thus on the spatial pattern of deforestation and the degree of land surface heterogeneity. Furthermore, we find that despite this region-wide suppression of shallow cumuli, the increased low-level moisture drives more of the shallow cumuli that do form to start raining earlier in the day. This leads to shifts in the diurnal timing and coverage of shallow precipitation, which motivates the need for further observational validation that disaggregates deforestation impacts on clouds and rainfall at different times of day (Leung et al., 2024; Ruijsch et al., 2025)

Deep convection is strongly impacted by deforestation-induced changes in large-scale moisture flux convergence. Deforestation dampens the land-ocean contrast in low-level temperatures, thereby weakening the sea breeze. This reduces moisture advection and limits development from shallow to deep convection, resulting in proportionally more clouds remaining as terminal congestus (4km<CTH<10km) instead of developing into deep convection (CTH>10km). The deep convection that does develop under the deforested scenario tends to now occur beyond sunset, with corresponding shifts in the diurnal precipitation maxima. Changes to diurnal timing may impact the net radiative effects of deep convective clouds and their anvils (Jones et al., 2024).

Compared to better-studied deforestation hotspots like the Amazon, the region of Southeast Asia we focus on here is unique both in terms of the prevailing land use (with the transition to oil palm and rubber plantations meaning evapotranspiration remains relatively high) and background meteorology (highly moist, with strong mesoscale influences on convection). We speculate the processes we discuss here are broadly applicable to other tropical deforestation regions with nearby moisture sources (e.g., Central America, coastal West Africa) (Kim et al., 2015; Taylor et al., 2022). That said, the *net* deforestation response is highly dependent on relative contributions from the local and regional processes we elucidate in this paper and thus may vary across regions and even seasons. For example, mesoscale breezes might become relatively more important compared to regional mean changes in boundary layer cloud development during the dry season (Leung et al., 2024). Deforestation impacts may further be modulated by other properties like aerosol emissions from forest clearing-related biomass burning (as visible in smoke in **Figure 1a,d**, but not included in our simulations). Such aerosol–land surface–cloud feedbacks have been shown to impact mesoscale circulations like the sea breeze (Grant and van den Heever 2014; Park and van den Heever 2022) and are the subject of a future set of planned investigations.

In conclusion, we demonstrate in this work that shallow and deep convection are coupled to the land surface through processes acting on different spatiotemporal scales. Shallow convection is more sensitive to deforestation-induced regional changes in thermodynamics and local changes in vegetation breezes, while deep convection is more sensitive to changes in moisture convergence associated with the sea breeze. There are strong diurnal structures and mesoscale heterogeneities in the signal of deforestation-driven changes in clouds and precipitation. Though typically unresolved in large-scale models, our findings emphasize that these convective and mesoscale processes must be carefully incorporated into assessments of the impacts of land cover changes on clouds, hydrology, and climate.

Acknowledgments

Funding was provided by the NASA Early Career Research program through FINESST 80NSSC22K1446. SCvdH acknowledges funding from NSF ESCAPE 2019947 and DOE TRACER DE-SC0021160. Computing resources supporting this work were provided by the NASA High-End Computing (HEC) program through the NASA Advanced Supercomputing (NAS) Division at Ames Research Center. We thank Dr. Aryeh Drager and Dr. Adele Igel for helpful discussions around the surface and radiation parameterizations used.

Open Research Section

Source code to reproduce the RAMS simulations are available at: https://doi.org/10.5281/zenodo.17055884 (Leung & Van Den Heever, 2025). Analysis and plotting code are available at: https://doi.org/10.5281/zenodo.17122475.

References

Argüeso, D., Romero, R., & Homar, V. (2020). Precipitation Features of the Maritime Continent in Parameterized and Explicit Convection Models. https://doi.org/10.1175/JCLI-D-19-0416.1

Ascher, B. D., Saleeby, S. M., Marinescu, P. J., & Heever, S. C. van den. (2025). Forest Breeze–Cold Pool Interactions Drive Convective Organization over Heterogeneous Vegetation. https://doi.org/10.1175/JAS-D-24-0084.1

Baidya Roy, S., & Avissar, R. (2002). Impact of land use/land cover change on regional hydrometeorology in Amazonia. *Journal of Geophysical Research: Atmospheres*, *107*(D20), LBA 4-1-LBA 4-12. https://doi.org/10.1029/2000JD000266

Boysen, L. R., Brovkin, V., Pongratz, J., Lawrence, D. M., Lawrence, P., Vuichard, N., et al. (2020). Global climate response to idealized deforestation in CMIP6 models. *Biogeosciences*, *17*(22), 5615–5638. https://doi.org/10.5194/bg-17-5615-2020

Chen, C.-C., Lo, M.-H., Im, E.-S., Yu, J.-Y., Liang, Y.-C., Chen, W.-T., et al. (2019). Thermodynamic and Dynamic Responses to Deforestation in the Maritime Continent: A Modeling Study. *Journal of Climate*, *32*(12), 3505–3527. https://doi.org/10.1175/JCLI-D-18-0310.1

Chen, H.-C., & Lo, M.-H. (2023). Contrasting Responses of Surface Heat Fluxes to Tropical Deforestation. *Journal of Geophysical Research: Atmospheres*, *128*(12), e2022JD038118. https://doi.org/10.1029/2022JD038118

Chen, J., Hagos, S., Xiao, H., Fast, J., & Feng, Z. (2023). Multiscale Analysis of Surface Heterogeneity–Induced Convection on Isentropic Coordinates. https://doi.org/10.1175/JAS-D-21-0198.1

Chen, S., Woodcock, C., Dong, L., Tarrio, K., Mohammadi, D., & Olofsson, P. (2024). Review of drivers of forest degradation and deforestation in Southeast Asia. *Remote Sensing Applications: Society and Environment*, *33*, 101129. https://doi.org/10.1016/j.rsase.2023.101129

Cioni, G., & Hohenegger, C. (2017). Effect of Soil Moisture on Diurnal Convection and Precipitation in Large-Eddy Simulations. *Journal of Hydrometeorology*, *18*(7), 1885–1903. https://doi.org/10.1175/JHM-D-16-0241.1

Cotton, W. R., Pielke Sr., R. A., Walko, R. L., Liston, G. E., Tremback, C. J., Jiang, H., et al. (2003). RAMS 2001: Current status and future directions. *Meteorology and Atmospheric Physics*, *82*(1). https://doi.org/10.1007/s00703-001-0584-9

Crompton, O., Corrêa, D., Duncan, J., & Thompson, S. (2021). Deforestation-induced surface warming is influenced by the fragmentation and spatial extent of forest loss in Maritime Southeast Asia. *Environmental Research Letters*, *16*(11), 114018. https://doi.org/10.1088/1748-9326/ac2fdc

Davin, E. L., & de Noblet-Ducoudré, N. de. (2010). Climatic Impact of Global-Scale Deforestation: Radiative versus Nonradiative Processes. *Journal of Climate*, *23*(1), 97–112. https://doi.org/10.1175/2009JCLI3102.1

Drager, A. J., Grant, L. D., & Heever, S. C. van den. (2020). Cold Pool Responses to Changes in Soil Moisture. *Journal of Advances in Modeling Earth Systems*, *12*(8), e2019MS001922. https://doi.org/10.1029/2019MS001922

Duveiller, G., Filipponi, F., Ceglar, A., Bojanowski, J., Alkama, R., & Cescatti, A. (2021). Revealing the widespread potential of forests to increase low level cloud cover. *Nature Communications*, *12*(1), 4337. https://doi.org/10.1038/s41467-021-24551-5

Falk, N. M., Leung, G. R., Grant, L. D., & Van Den Heever, S. C. (2025). Cold pools reduce the impacts of deforestation on convective initiation.

FAO United Nations. (1974). Soil map of the world. Paris: Unesco.

Findell, K. L., & Eltahir, E. A. B. (2003). Atmospheric Controls on Soil Moisture–Boundary Layer Interactions. Part I: Framework Development. *Journal of Hydrometeorology*, *4*(3), 552–569. https://doi.org/10.1175/1525-7541(2003)004%253C0552:ACOSML%253E2.0.CO;2

Fowler, D., Nemitz, E., Misztal, P., Di Marco, C., Skiba, U., Ryder, J., et al. (2011). Effects of land use on surface–atmosphere exchanges of trace gases and energy in Borneo: comparing fluxes over oil palm plantations and a rainforest. *Philosophical Transactions of the Royal Society B: Biological Sciences*, *366*(1582), 3196–3209. https://doi.org/10.1098/rstb.2011.0055

Friedl, M. A., McIver, D. K., Hodges, J. C. F., Zhang, X. Y., Muchoney, D., Strahler, A. H., et al. (2002). Global land cover mapping from MODIS: algorithms and early results. *Remote Sensing of Environment*, *83*(1), 287–302. https://doi.org/10.1016/S0034-4257(02)00078-0

Gentine, P., Holtslag, A. A. M., D'Andrea, F., & Ek, M. (2013). Surface and Atmospheric Controls on the Onset of Moist Convection over Land. *Journal of Hydrometeorology*, *14*(5), 1443–1462. https://doi.org/10.1175/JHM-D-12-0137.1

Gentine, P., Massmann, A., Lintner, B. R., Hamed Alemohammad, S., Fu, R., Green, J. K., et al. (2019). Land–atmosphere interactions in the tropics – a review. *Hydrology and Earth System Sciences*, *23*(10), 4171–4197. https://doi.org/10.5194/hess-23-4171-2019

Gero, A. F., & Pitman, A. J. (2006). The Impact of Land Cover Change on a Simulated Storm Event in the Sydney Basin. *Journal of Applied Meteorology and Climatology*, *45*(2), 283–300. https://doi.org/10.1175/JAM2337.1

Giambelluca, T. W., Mudd, R. G., Liu, W., Ziegler, A. D., Kobayashi, N., Kumagai, T., et al. (2016). Evapotranspiration of rubber (Hevea brasiliensis) cultivated at two plantation sites in Southeast Asia. *Water Resources Research*, *52*(2), 660–679. https://doi.org/10.1002/2015WR017755

Grant, L. D., & van den Heever, S. C. (2014). Aerosol-cloud-land surface interactions within tropical sea breeze convection. *Journal of Geophysical Research: Atmospheres*, *119*(13), 8340–8361. https://doi.org/10.1002/2014JD021912

Hardwick, S. R., Toumi, R., Pfeifer, M., Turner, E. C., Nilus, R., & Ewers, R. M. (2015). The relationship between leaf area index and microclimate in tropical forest and oil palm plantation: Forest disturbance drives changes in microclimate. *Agricultural and Forest Meteorology*, *201*, 187–195. https://doi.org/10.1016/j.agrformet.2014.11.010

Heikenfeld, M., Marinescu, P. J., Christensen, M., Watson-Parris, D., Senf, F., van den Heever, S. C., & Stier, P. (2019). tobac 1.2: towards a flexible framework for tracking and analysis of clouds in diverse datasets. *Geoscientific Model Development*, *12*(11), 4551–4570. https://doi.org/10.5194/gmd-12-4551-2019

Hersbach, H., Bell, B., Berrisford, P., Hirahara, S., Horányi, A., Muñoz-Sabater, J., et al. (2020). The ERA5 global reanalysis. *Quarterly Journal of the Royal Meteorological Society*, *146*(730), 1999–2049. https://doi.org/10.1002/qj.3803

Hill, G. E. (1974). Factors Controlling the Size and Spacing of Cumulus Clouds as Revealed by Numerical Experiments. Retrieved from https://journals.ametsoc.org/view/journals/atsc/31/3/1520-0469_1974_031_0646_fctsas_2_0_co_2.xml

Jamaludin, J., De Alban, J. D. T., Carrasco, L. R., & Webb, E. L. (2022). Spatiotemporal analysis of deforestation patterns and drivers reveals emergent threats to tropical forest landscapes. *Environmental Research Letters*, *17*(5), 054046. https://doi.org/10.1088/1748-9326/ac68fa

Johnson, R. H., Rickenbach, T. M., Rutledge, S. A., Ciesielski, P. E., & Schubert, W. H. (1999). Trimodal Characteristics of Tropical Convection. *Journal of Climate*, *12*, 22.

Jones, W. K., Stengel, M., & Stier, P. (2024). A Lagrangian perspective on the lifecycle and cloud radiative effect of deep convective clouds over Africa. *Atmospheric Chemistry and Physics*, *24*(9), 5165–5180. https://doi.org/10.5194/acp-24-5165-2024

June, T., Meijide, A., Stiegler, C., Kusuma, A. P., & Knohl, A. (2018). The influence of surface roughness and turbulence on heat fluxes from an oil palm plantation in Jambi, Indonesia. *IOP Conference Series: Earth and Environmental Science*, *149*(1), 012048. https://doi.org/10.1088/1755-1315/149/1/012048

Khanna, J., Medvigy, D., Fueglistaler, S., & Walko, R. (2017). Regional dry-season climate changes due to three decades of Amazonian deforestation. *Nature Climate Change*, *7*(3), 200–204. https://doi.org/10.1038/nclimate3226

Kim, D.-H., Sexton, J. O., & Townshend, J. R. (2015). Accelerated deforestation in the humid tropics from the 1990s to the 2000s. *Geophysical Research Letters*, *42*(9), 3495–3501. https://doi.org/10.1002/2014GL062777

Laguë, M. M., Swann, A. L. S., & Boos, W. R. (2021). Radiative Feedbacks on Land Surface Change and Associated Tropical Precipitation Shifts. *Journal of Climate*, *34*(16), 6651–6672. https://doi.org/10.1175/JCLI-D-20-0883.1

Leung, G. R., & van den Heever, S. C. (2022). Controls on the Development and Circulation of Terminal versus Transient Congestus Clouds and Implications for Midlevel Aerosol Transport. *Journal of the Atmospheric Sciences*, *79*(11), 3083–3101. https://doi.org/10.1175/JAS-D-21-0314.1

Leung, G. R., & Van Den Heever, S. C. (2025, September 4). grleung/rams: RAMS Borneo LCC Simulations (Version borneolcc-paper). Zenodo. Retrieved from https://doi.org/10.5281/zenodo.17055884

Leung, G. R., Grant, L. D., & van den Heever, S. C. (2024). Deforestation-Driven Increases in Shallow Clouds Are Greatest in Drier, Low-Aerosol Regions of Southeast Asia. *Geophysical Research Letters*, *51*(10), e2023GL107678. https://doi.org/10.1029/2023GL107678

Lilly, D. K. (1962). On the numerical simulation of buoyant convection. *Tellus*, *14*(2), 148–172. https://doi.org/10.1111/j.2153-3490.1962.tb00128.x

Luo, Z., Liu, G. Y., Stephens, G. L., & Johnson, R. H. (2009). Terminal versus transient cumulus congestus: A CloudSat perspective. *Geophysical Research Letters*, *36*(5). https://doi.org/10.1029/2008GL036927

Mahmood, R., Pielke Sr., R. A., Hubbard, K. G., Niyogi, D., Dirmeyer, P. A., McAlpine, C., et al. (2014). Land cover changes and their biogeophysical effects on climate. *International Journal of Climatology*, *34*(4), 929–953. https://doi.org/10.1002/joc.3736

Marzuki, M., Yusnaini, H., Ramadhan, R., Tangang, F., Amirudin, A. A. B., Hashiguchi, H., et al. (2022). Characteristics of Precipitation Diurnal Cycle over a Mountainous Area of Sumatra Island including MJO and Seasonal Signatures Based on the 15-Year Optical Rain Gauge Data, WRF Model and IMERG. *Atmosphere*, *13*(1), 63. https://doi.org/10.3390/atmos13010063

Meyers, M. P., Walko, R. L., Harrington, J. Y., & Cotton, W. R. (1997). New RAMS cloud microphysics parameterization. Part II: The two-moment scheme. *Atmospheric Research*, *45*(1), 3–39. https://doi.org/10.1016/S0169-8095(97)00018-5

van der Molen, M. K., Dolman, A., Waterloo, M., & Bruijnzeel, L. (2006). Climate is affected more by maritime than by continental land use change: A multiple scale analysis. *Global and Planetary Change*, *54*(1–2), 128–149. https://doi.org/10.1016/j.gloplacha.2006.05.005

Parker, D., Tosiani, A., Yazid, M., Sari, I. L., Kartika, T., Kustiyo, et al. (2024). Land in limbo: Nearly one third of Indonesia's cleared old-growth forests left idle. *Proceedings of the National Academy of Sciences*, *121*(28), e2318029121. https://doi.org/10.1073/pnas.2318029121

Pielke Sr., R.A., Cotton, W. R., Walko, R. L., Tremback, C. J., Lyons, W. A., Grasso, L. D., et al. (1992). A comprehensive meteorological modeling system—RAMS. *Meteorology and Atmospheric Physics*, *49*(1), 69–91. https://doi.org/10.1007/BF01025401

Pielke Sr., Roger A. (2001). Influence of the spatial distribution of vegetation and soils on the prediction of cumulus Convective rainfall. *Reviews of Geophysics*, *39*(2), 151–177. https://doi.org/10.1029/1999RG000072

Pincus, R., Mlawer, E. J., & Delamere, J. S. (2019). Balancing Accuracy, Efficiency, and Flexibility in Radiation Calculations for Dynamical Models. *Journal of Advances in Modeling Earth Systems*, *11*(10), 3074–3089. https://doi.org/10.1029/2019MS001621

Qian, J.-H. (2008). Why Precipitation Is Mostly Concentrated over Islands in the Maritime Continent. *Journal of the Atmospheric Sciences*, *65*(4), 1428–1441. https://doi.org/10.1175/2007JAS2422.1

Reid, J. S., Maring, H. B., Narisma, G. T., Heever, S. van den, Girolamo, L. D., Ferrare, R., et al. (2023). The coupling between tropical meteorology, aerosol lifecycle, convection, and radiation, during the Cloud, Aerosol and Monsoon Processes Philippines Experiment (CAMP2Ex). *Bulletin of the American Meteorological Society*, *1*(aop). https://doi.org/10.1175/BAMS-D-21-0285.1

Renggono, F., Hashiguchi, H., Fukao, S., Yamanaka, M. D., Ogino, S.-Y., Okamoto, N., et al. (2001). Precipitating clouds observed by 1.3-GHz boundary layer radars in equatorial Indonesia. *Annales Geophysicae*, *19*(8), 889–897. https://doi.org/10.5194/angeo-19-889-2001

Rieck, M., Hohenegger, C., & Heerwaarden, C. C. van. (2014). The Influence of Land Surface Heterogeneities on Cloud Size Development. *Monthly Weather Review*, *142*(10), 3830–3846. https://doi.org/10.1175/MWR-D-13-00354.1

Ruijsch, J., Taylor, C. M., Hutjes, R. W. A., & Teuling, A. J. (2025). Scale-dependent cloud enhancement from land restoration in West African drylands. *Communications Earth & Environment*, *6*(1), 1–11. https://doi.org/10.1038/s43247-025-02154-y

Saad, S. I., Rocha, H. R. da, Dias, M. A. F. S., & Rosolem, R. (2010). Can the Deforestation Breeze Change the Rainfall in Amazonia? A Case Study for the BR-163 Highway Region. *Earth Interactions*. https://doi.org/10.1175/2010EI351.1

Sabajo, C. R., le Maire, G., June, T., Meijide, A., Roupsard, O., & Knohl, A. (2017). Expansion of oil palm and other cash crops causes an increase of land surface temperature in Indonesia. *Biogeosciences*. https://doi.org/10.5194/bg-2017-203

Saleeby, S. M., & Cotton, W. R. (2008). A Binned Approach to Cloud-Droplet Riming Implemented in a Bulk Microphysics Model. *Journal of Applied Meteorology and Climatology*, *47*(2), 694–703.

Saleeby, S. M., & van den Heever, S. C. (2013). Developments in the CSU-RAMS Aerosol Model: Emissions, Nucleation, Regeneration, Deposition, and Radiation. *Journal of Applied Meteorology and Climatology*, *52*(12), 2601–2622. https://doi.org/10.1175/JAMC-D-12-0312.1

Santanello, J. A., Dirmeyer, P. A., Ferguson, C. R., Findell, K. L., Tawfik, A. B., Berg, A., et al. (2018). Land–Atmosphere Interactions: The LoCo Perspective. *Bulletin of the American Meteorological Society*, *99*(6), 1253–1272. https://doi.org/10.1175/BAMS-D-17-0001.1

Schneck, R., & Mosbrugger, V. (2011). Simulated climate effects of Southeast Asian deforestation: Regional processes and teleconnection mechanisms. *Journal of Geophysical Research: Atmospheres*, *116*(D11). https://doi.org/10.1029/2010JD015450

Smagorinsky, J. (1963). General Circulation Experiments with the Primitive Equations. *Monthly Weather Review*. https://doi.org/10.1175/1520-0493(1963)091%3C0099:GCEWTP%3E2.3.CO;2

Sokolowsky, G. A., Freeman, S. W., Jones, W. K., Kukulies, J., Senf, F., Marinescu, P. J., et al. (2024). *tobac* v1.5: introducing fast 3D tracking, splits and mergers, and other enhancements for identifying and analysing meteorological phenomena. *Geoscientific Model Development*, *17*(13), 5309–5330. https://doi.org/10.5194/gmd-17-5309-2024

Spracklen, D. V., Baker, J. C. A., Garcia-Carreras, L., & Marsham, J. H. (2018). The Effects of Tropical Vegetation on Rainfall. *Annual Review of Environment and Resources*, *43*(1), 193–218. https://doi.org/10.1146/annurev-environ-102017-030136

Stull, R. B. (1988). Boundary Layer Clouds. In R. B. Stull (Ed.), *An Introduction to Boundary Layer Meteorology* (pp. 545–585). Dordrecht: Springer Netherlands. https://doi.org/10.1007/978-94-009-3027-8_13

Takahashi, A., Kumagai, T., Kanamori, H., Fujinami, H., Hiyama, T., & Hara, M. (2017). Impact of Tropical Deforestation and Forest Degradation on Precipitation over Borneo Island. *Journal of Hydrometeorology*, *18*(11), 2907–2922. https://doi.org/10.1175/JHM-D-17-0008.1

Takanashi, S., Kosugi, Y., Ohkubo, S., Matsuo, N., Tani, M., & Nik, A. R. (2010). Water and heat fluxes above a lowland dipterocarp forest in Peninsular Malaysia. *Hydrological Processes*, *24*(4), 472–480. https://doi.org/10.1002/hyp.7499

Tang, A. C. I., Stoy, P. C., Hirata, R., Musin, K. K., Aeries, E. B., Wenceslaus, J., et al. (2019). The exchange of water and energy between a tropical peat forest and the atmosphere: Seasonal trends and comparison against other tropical rainforests. *Science of The Total Environment*, *683*, 166–174. https://doi.org/10.1016/j.scitotenv.2019.05.217

Taylor, C. M., Klein, C., Parker, D. J., Gerard, F., Semeena, V. S., Barton, E. J., & Harris, B. L. (2022). “Late-stage” deforestation enhances storm trends in coastal West Africa. *Proceedings of the National Academy of Sciences*, *119*(2), e2109285119. https://doi.org/10.1073/pnas.2109285119

Tölle, M. H., Engler, S., & Panitz, H.-J. (2017). Impact of Abrupt Land Cover Changes by Tropical Deforestation on Southeast Asian Climate and Agriculture. *Journal of Climate*, *30*(7), 2587–2600. https://doi.org/10.1175/JCLI-D-16-0131.1

Walko, R. L., Band, L. E., Baron, J., Kittel, T. G. F., Lammers, R., Lee, T. J., et al. (2000). Coupled Atmosphere–Biophysics–Hydrology Models for Environmental Modeling. *Journal of Applied Meteorology and Climatology*, *39*(6), 931–944. https://doi.org/10.1175/1520-0450(2000)039%253C0931:CABHMF%253E2.0.CO;2

Werth, D., & Avissar, R. (2005). The local and global effects of Southeast Asian deforestation. *Geophysical Research Letters*, *32*(20). https://doi.org/10.1029/2005GL022970

Winkler, K., Fuchs, R., Rounsevell, M., & Herold, M. (2021). Global land use changes are four times greater than previously estimated. *Nature Communications*, *12*(1), 2501. https://doi.org/10.1038/s41467-021-22702-2

Xu, R., Li, Y., Teuling, A. J., Zhao, L., Spracklen, D. V., Garcia-Carreras, L., et al. (2022). Contrasting impacts of forests on cloud cover based on satellite observations. *Nature Communications*, *13*(1), 670. https://doi.org/10.1038/s41467-022-28161-7

Yang, G.-Y., & Slingo, J. (2001). The Diurnal Cycle in the Tropics. *Monthly Weather Review*. https://doi.org/10.1175/1520-0493(2001)129%3C0784:TDCITT%3E2.0.CO;2